Max-Planck-Institut
für Mathematik
in den Naturwissenschaften
Leipzig

Emerging patterns in a hyperbolic model for locally interacting cell systems

by

Frithjof Lutscher and Angela Stevens

Preprint no.: 98 2001

Emerging patterns in a hyperbolic model for locally interacting cell systems

Frithjof Lutscher*
Biomathematik
Universität Tübingen
Germany

Angela Stevens†
Max-Planck-Institute for
Mathematics in the Sciences
Leipzig, Germany

Abstract

Morphogenetic processes like, for example, neurulation and gastrulation involve coordinated movements of cells. It is assumed that these processes happen due to long range signaling, although the detailed mechanisms are not completely understood. Therefore, one is interested in biological "model-systems" where self-organization of cells and in particular the mechanisms of signaling can be analyzed in greater detail. A major question is whether or not also short range signaling or local interaction of cells can be the cause of coordinated movement and morphogenetic processes. As a model problem we analyze ripple formation of myxobacteria due to purely local interaction, a hypothesis which is discussed in the biological literature. These ripples can be observed before the final aggregation of the bacteria and fruiting body formation takes place.

Our basic mathematical model is a one-dimensional hyperbolic system of Goldstein-Kac type with density dependent coefficients. Conditions for the existence of traveling waves are discussed by means of linear analysis and the construction of invariant domains.

1 Introduction

Myxobacteria are ubiquitous soil bacteria which show several forms of social behavior. Vegetative cells evolve from myxospores and grow under suitable conditions. The bacteria are elongated cells which glide in the direction of their long axis. They produce slime trails on which they prefer to move. They may also move faster on these trails. During their movement they can stop, and then either reverse or choose a new direction. Individual cells form groups in

*flutscher@math.ualberta.ca. Present address: Department for Mathematical and Statistical Sciences, University of Alberta, Edmonton, AB, Canada T6G 2G1. Partially supported by the Max-Planck-Institute for Mathematics in the Sciences, Leipzig

†stevens@mis.mpg.de, partially supported by the Research Institute for Mathematics in the Sciences, Kyoto University, 606-8502 Kyoto, Japan.

which they align their long axes in approximately the same direction and move in swarms and streets. Under starvation conditions the cells aggregate, and several kinds of patterns can be observed. Finally, fruiting bodies are formed which lift off the two dimensional surface. Within these fruiting bodies myxospores are formed, waiting dormantly for appropriate external conditions to restart the developmental cycle.

In the laboratory, one can often observe a long phase of *rippling* behavior before the onset of aggregation. We summarize the results in [19]: 'The observable pattern consists of a series of equally spaced ridges which move as traveling waves. It covers large areas but does not spread. It can last for days but still there is no net transport of cells. Two ripples interpenetrate one another without interference. The long axes of cells within ripples and particularly at ripple crests are oriented approximately perpendicular to the movement direction of the crest.'

A great deal of biological research has been devoted to the study of intercellular signaling and coordinated movement in order to explain the observed social behavior. C-factor is one of several different extracellular signals which have been identified as playing a major role during this process. In contrast to A-factor, which is known to diffuse, C-factor is bound to the cell surface [13] and hence its transmission requires cell contact. It was shown that C-factor is best transmitted in end-to-end contact of cells which form, at most, an obtuse angle [13]. Sager and Kaiser propose the following mechanism for rippling in [19]: End-to-end collision between cells initiates C-signaling, which in turn increases the reversal probability of individual cells. If two ripple crests meet, they reflect one another point by point such that the overall shape travels on. Individual cells, however, move back and forth on the order of one wavelength (on average) and reverse direction upon contact with countermigrating cells. A somewhat similar phenomenon is found in water waves where the shape of the wave travels, but single drops merely move back and forth.

Evidence for this hypothesis comes from the following experimental results given in [19]: Artificial addition of C-factor increases reversal in cell cultures. Cells in ripple crests have a higher reversal frequency than in troughs. Mutant cells ($csgA^-$) that are incapable of C-signaling but respond to C-factor were introduced into the cell culture. As the proportion of $csgA^-$ increased, the ripple wavelength and width increased, and the ripple velocity remained constant. If the fraction of $csgA^-$ exceeded 90%, cells did not show rippling any more. Another mutant type (*frz*) is known to be unable to ripple. It had been shown that these mutants have a very low (*frz*A,B,C,E,F) or very high (*frz*D) reversal frequency compared to the wild type [1].

If rippling would be a phenomenon comparable to the behavior of coupled oscillators, then these mutants should also show rippling behavior, but possibly at different frequencies. Therefore, Sager and Kaiser suggested that the C-signaling in *frz*-mutants is decoupled from cell movement. Finally, by the use of fluorescence markers, they followed paths of individual cells in ripples. They found that single cells moved back and forth while the ripple crest moved over the whole area of observation.

In this paper we present a hyperbolic model for the effect of local interaction on individual movement and apply it to the rippling phenomenon as described above. The model is simple in that the only mechanism we assume is that end-to-end contact of cells triggers cell reversal. Before we formulate the model, however, we have a closer look at the behavior of a single cell when two ripple crests meet (Figure 1). Black cells move to the left, white ones to the right. We follow the grey cell which initially moves right and is a little ahead of the right moving crest. As it comes into contact with countermigrating (black) cells it reverses direction. Then it is ahead of the left moving crest and should reverse upon contact with the white right moving cells. In a grid point model described in [2] it was assumed that after C-signaling has induced the reversal of cells they undergo a rest phase during which they do not respond to the signal. During this "insensitive phase" the grey cell, after the first reversal, would "tunnel" through the right moving crest without reversing direction. It could then travel one wavelength and reverse direction again once it has encountered the next crest. The duration of the insensitive phase influences the wavelength of ripples. A similar idea is used in [11]. The ratio of the length of the insensitive and sensitive phase has to be tuned well to get the rippling pattern.

Here we propose a different model which does not make any assumptions about an insensitive phase. The grey cell in between the two countermigrating ripple crests reverses its direction frequently, namely, upon encountering cells from an oncoming crest. Once the crests have passed, the shapes travel on whereas the formerly white cells now move to the left and the formerly black ones to the right, and the grey cell can continue its path. Thus, in the model presented here, a single cell will typically not move one wavelength and then reverse, but will have a more complicated path. On average, however, cells will move one wavelength in one direction.

Various mathematical models for the gliding behavior and aggregation of myxobacteria have been derived and studied. In [20, 21, 23] a two-dimensional grid point model for trail following and final aggregation due to a diffusing signal was simulated (compare also the last section in this paper). This model was set into context with an interacting stochastic many particle system, from which parabolic continuum equations for the dynamics of the cell density were

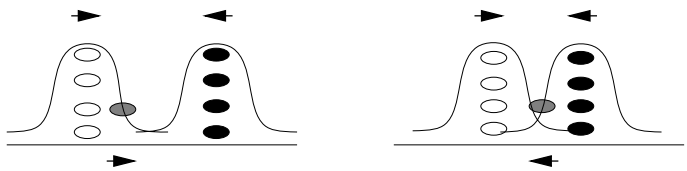

Figure 1: Two countermigrating ripple crests meet. The grey cell initially moves to the right (left plot), then reverses direction due to an encounter with (black) left moving cells. Later it will have a new encounter with (white) right moving cells (right plot).

derived, [22]. In [18], a one-dimensional integro-differential equation system was considered to model the swarming behavior of myxobacteria. Bacteria move on the line either to the right or to the left with average speed γ. The density of cells $u = u(t, x)$ is split accordingly into the right and left moving fraction $u^{\pm}$. Bacteria are assumed to have a perception range of length $2R$ in a neighborhood of their position. They change direction with rates $\mu^{\pm}$ which are dependent on the densities in the perception interval. The resulting model is the following system of hyperbolic equations.

$$\begin{aligned} u_t^+ + \gamma u_x^+ &= -\mu^+ u^+ + \mu^- u^-, \\ u_t^- - \gamma u_x^- &= \mu^+ u^+ - \mu^- u^-, \end{aligned} \tag{1}$$

where the turning frequencies are defined for a function F and weight functions α, β as follows

$$\mu^{\pm} = F\left(\int_{-R}^{R} \alpha(r) u^{\pm}(t, x \pm r) + \beta(r) u^{\mp}(t, x \pm r) dr\right).$$

The model is non-local in space. To obtain a local model, the integrals are approximated by local Taylor series. With this approximation, the turning rates are functions of the densities $u^{\pm}$ and their gradients $u_x^{\pm}$. It is not known whether cells can perceive such population density gradients. It was argued, for example, that myxobacteria move too slowly to detect gradients of chemical signals [17].

A two-dimensional model for cell orientation due to cell-cell interaction (i.e., surface bound signals) was derived and investigated in [3, 4]. A detailed bifurcation analysis yielded a rich variety of patterns that can evolve depending on the interaction. Movement in space, however, was not considered.

If $\mu = \mu^+ = \mu^- = constant$, system (1) is the Goldstein-Kac model for a correlated random walk [12]. This system was a starting point for many models of spatial spread, interaction, alignment and chemotaxis of biological species [6, 7, 9, 10, 16]. Here we generalize this model. We consider (1) with turning rates depending pointwise on the densities, since we want to analyze the possible effects of purely local interaction. The qualitative analysis of the model is done by linear stability analysis, the construction of invariant domains and by determining limit sets. It is shown that the model supports traveling wavetrains in opposite directions and hence is capable of describing rippling behavior in myxobacteria. Numerical simulations of rippling behavior are given for various choices of turning rates. Finally, the model is also applied to describe the formation of aggregates. Slight changes in the parameter values switch the system from one behavior to the other.

2 The one dimensional hyperbolic model

We start with a model of Goldstein-Kac type where the turning rates are allowed to depend on the densities of the right and left moving populations. We

distinguish between autonomous turning and turning induced by interaction. The model reads

$$\begin{aligned} u_t^+ + \gamma u_x^+ &= -(\mu + \lambda^+)u^+ + (\mu + \lambda^-)u^-, \\ u_t^- - \gamma u_x^- &= (\mu + \lambda^+)u^+ - (\mu + \lambda^-)u^-, \end{aligned} \tag{2}$$

where $\mu > 0$ is the rate of autonomous turning and $\lambda^\pm = \lambda^\pm(u^+, u^-) \geq 0$ are the turning rates due to interaction. In the notation of (1) the total turning rates are $\mu^\pm = \mu + \lambda^\pm$. But here the rates depend pointwise on the cell densities. Naturally, the interaction process can be assumed symmetric with respect to interchanging left and right, therefore we have

$$\lambda^+(u^+, u^-) = \lambda^-(u^-, u^+) =: \lambda(u^+, u^-). \tag{3}$$

We impose Neumann boundary conditions on the interval $[0, l]$:

$$u^+(t, x) = u^-(t, x) \qquad \text{for} \qquad x \in \{0, l\}. \tag{4}$$

These conditions reflect the observation that rippling patterns can form over the entire surface of a developing mat [19]. Also, if rippling patterns evolve only locally, then they do not spread in time. In the second case, ideally, one would include into the model conditions of how cells behave as soon as they glide at the edge of the colony. Since no biological details are known about cell behavior at the edges, we do not consider this problem here.

System (2) preserves positivity for $u^\pm$. Furthermore, the total density $u = u^+ + u^-$ satisfies $u_t + \gamma v_x = 0$, where $v = u^+ - u^-$ denotes the flux. Hence, the total density is preserved. In [15, 16] a system similar to (2) was derived and investigated with respect to alignment of individuals. Some of the proofs presented there can be carried over to our model. In particular, we get the following existence result.

Theorem 2.1 *Let the turning rates $\mu^\pm : \mathbb{R}_+^2 \to \mathbb{R}$ be continuously differentiable with locally Lipschitz continuous first partial derivatives. Then for all initial data $u^\pm \in \mathcal{C}^1([0, l])$ which satisfy the compatibility conditions (4) there exists a unique solution*

$$(u^+, u^-) \in \mathcal{C}^1([0, T) \times [0, l])^2$$

of (2), (4) for some time $T > 0$. Furthermore, system (2) on $[0, l]$ with boundary conditions (4) is equivalent to system (2) on $[0, 2l]$ with periodic boundary conditions, i.e., $u^\pm(t, 0) = u^\pm(t, 2l)$, and the initial symmetry condition $u^+(0, x) = u^-(0, 2l - x)$, which is preserved in time.

The stationary states of (2), (4) are given by $u^+ = u^- = c =$const. Defining $u^\pm = c + w^\pm$ we obtain a linear system for the perturbations $w^\pm$:

$$\begin{aligned} w_t^+ + \gamma w_x^+ &= [\mu + \lambda(c, c) + \partial_1\lambda(c, c)c - \partial_2\lambda(c, c)c](w^- - w^+), \\ w_t^- - \gamma w_x^- &= [\mu + \lambda(c, c) + \partial_1\lambda(c, c)c - \partial_2\lambda(c, c)c](w^+ - w^-). \end{aligned} \tag{5}$$

Lemma 2.2 *A stationary solution $u^{\pm} = c > 0$ of (2) is linearly stable if and only if*

$$\Lambda := \mu + \lambda(c,c) + \partial_1\lambda(c,c)c - \partial_2\lambda(c,c)c > 0. \tag{6}$$

At the bifurcation point all eigenvalues cross the imaginary axis.

Proof. Setting $w = w^+ + w^-$ and using the so-called "Kac trick" [5] one can reduce (5) to the single equation

$$w_{tt} + 2\Lambda w_t = \gamma^2 w_{xx}.$$

Hence, the state $u^{\pm} = c$ is stable if $2\Lambda w_t$ is a damping term, i.e., if $\Lambda > 0$. ■

Remark:
From the stability condition (6) we get an explanation as to why mutant cells with high autonomous reversal frequencies do not show rippling behavior. Suppose that these mutants react to C-factor in the same way as the wild type does, i.e., according to the same λ. Then for increasing μ condition (6) will eventually be satisfied and hence the homogeneous stationary state is stable, so no patterns evolve.

During the rippling phase of myxobacteria one can observe that cell densities stay well below the densities found in aggregation centers before stalk formation. In our model we find an upper bound for the cell densities $u^{\pm}$, which depends on the specific interaction kinetics.

Lemma 2.3 *The domain $[0,s]^2$ is invariant for the system (2) if*

$$\frac{\lambda(w,s)w - \lambda(s,w)s}{s-w} \le \mu \quad \text{for} \quad 0 \le w \le s. \tag{7}$$

Proof. Application of the invariance principle in [8]. ■

Now we combine our results in order to obtain conditions on the qualitative behavior of the turning function λ such that $[0,s]^2$ is invariant for (2) and at the same time $u^{\pm} = c$ is unstable for

$$0 < c_1 < c < c_2 < s. \tag{8}$$

This will give a hint as to when traveling wavetrains might occur. First, we rewrite (7) as follows:

$$I(w) : = \mu(w-s) + \lambda(w,s)w - \lambda(s,w)s \le 0 \quad \text{for} \quad 0 \le w \le s. \tag{9}$$

Note that $I(0) = -\mu s - \lambda(s,0)s < 0$ and $I(s) = 0$. If (9) is to be satisfied in a neighborhood of s then $I'(s) \ge 0$, which is

$$\mu + \lambda(s,s) + \partial_1\lambda(s,s)s - \partial_2\lambda(s,s)s \ge 0,$$

which is the stability condition (6) for $c = s$. So, if $[0, s]^2$ is invariant then $u^{\pm} = s$ cannot be unstable. For the invariance condition to be satisfied it suffices that (9) holds for all maxima of I. The condition $I'(w_0) = 0$ substituted into (9) results in

$$-\mu s - \lambda(s, w_0)s - \partial_1\lambda(w_0, s)w_0^2 + \partial_2\lambda(s, w_0)sw_0 \leq 0. \tag{10}$$

2.1 Two examples of possible turning functionals

Formulating the model above, we allowed for general turning functions $\lambda^{\pm}$. Now we specify some properties of these turning functions. These properties reflect the biological hypotheses described in the introduction. Since turning is induced by C-factor, and C-factor is best transmitted by end-to-end contact of cells [13], we first investigate the case that λ^+ depends only on u^-, i.e., the turning rate for right moving cells depends only on the density of left moving cells. Like many other phenomena of coordinated behavior in myxobacteria, rippling may depend on the total mass of bacteria [13]. Therefore, in a second step we consider the case that λ^+ depends on u^- and the total density $u = u^+ + u^-$.

Case 1: $\lambda(u^+, u^-) = f(u^-)$
The state $u^{\pm} = c$ is unstable if

$$\mu + f(c) - f'(c)c < 0, \tag{11}$$

and the domain $[0, s]^2$ is invariant if for $0 \leq w \leq s$ we have

$$\mu(w - s) + f(s)w - f(w)s \leq 0. \tag{12}$$

From (11) we see that for $u^{\pm} = c$ close to zero, the homogeneous state is always stable as long as $f'(0)$ is bounded. This behavior corresponds well to the fact that a critical mass of cells is required for rippling to occur. Instability of $u^{\pm} = c$ for $c \in (c_1, c_2)$ requires $f'(c) > \frac{f(c)+\mu}{c}$. Let g fulfill

$$g'(c) = \frac{g(c) + \mu}{c} \quad \text{for} \quad c \in (c_1, c_2) \quad \text{and} \quad g(c_1) = f(c_1). \tag{13}$$

Then $g \leq f$. Solving the equality we obtain

$$f(c) \geq g(c) = \mu\left(\frac{c}{c_1} - 1\right) + \frac{f(c_1)}{c_1}c \tag{14}$$

or respectively

$$(\mu + f(c))c_1 \geq (\mu + f(c_1))c. \tag{15}$$

Hence f must be superlinear in the interval of instability (c_1, c_2).

The invariance condition (12) can be rewritten as

$$(\mu + f(s))w \leq (\mu + f(w))s \tag{16}$$

and is supposed to hold for $0 \leq w \leq s$ for s sufficiently large. Since the right hand side of (16) is linear in s we see that f must be sublinear for large arguments. In the critical case $f(u^-) = u^-$ the interaction terms cancel and (2) becomes the simple Goldstein-Kac model. We see that f does not need to saturate or be bounded in order for the model to have invariant domains.

Case 2: $\lambda(u^+, u^-) = a(u)f(u^-)$
We extend Case 1 by allowing the turning rate to depend on the total density $u = u^+ + u^-$ with $a > 0$. We assume a separation of variables. The instability condition becomes

$$\frac{\mu}{a(2c)} + f(c) - f'(c)c < 0, \tag{17}$$

and the invariant condition reads

$$\mu(w - s) + a(w + s)\left[f(s)w - f(w)s\right] \leq 0 \qquad \text{for} \qquad 0 \leq w \leq s. \tag{18}$$

In this case we "split" the two effects of instability and invariance: We choose f as to satisfy (17) according to the superlinearity condition from Case 1 above with $\mu/a(2c)$ instead of μ. Then, by choosing $a(u)$ small enough for $u > s$ we can ensure (18) to hold. (Of course, the choices of a and f are not independent.)

In a different setting, system (2) was derived with $\lambda(u^+, u^-) = a(u)f(u^-)$ and $f(u^-) = (u^-)^2$ [15, 16]. The equations then read

$$\begin{aligned} u_t^+ + \gamma u_x^+ &= M(u^+, u^-)(u^- - u^+), \\ u_t^- - \gamma u_x^- &= M(u^+, u^-)(u^+ - u^-), \end{aligned} \tag{19}$$

where the net turning rate is given by $M(u^+, u^-) = \mu - a(u)u^+u^-$. By using an appropriate Lyapunov functional in case $\mu = 0$ the following was shown.

Lemma 2.4 *Consider system (19) with Neumann boundary conditions. Suppose $\mu = 0$ and $a(u) > 0$. If $(u^+, u^-) \in L^\infty$ is in some ω-limit set, then the right hand side of (19) vanishes a.e.*

If the right hand side of (19) vanishes a.e. then the density profiles of $u^\pm$ are simply traveling to the right and left with constant speed γ. In order for the right hand side of (19) to vanish a.e. we see that for almost all x in $[0, l]$ we must have $u^+(x), u^-(x) \in \{0, C\}$ for some $C > 0$, i.e., $u^\pm$ assume, at most, one nonzero value. A similar result for $\mu > 0$ could not be proven, but simulations (see next section) suggest that on limit sets we have $u^+(x), u^-(x) \in \{C_1, C_2\}$ for some $C_{1,2} > 0$, i.e., $u^\pm$ assume, at most, two different values. These values are given by the condition $M(C_1, C_2) = 0$. These spatially piecewise constant functions, traveling at speeds $\pm\gamma$, are weak solutions of (19) in the sense of conservation laws [14]. Hence, the model does support rippling-like patterns. We consider a particular choice of a in detail. Motivated by the modeling assumptions in [15, 16], the special case $a(u) = a_*/(1 + u^3)$ was studied. In this case, the existence of invariant domains was shown.

Lemma 2.5 *Consider system (19) with Neumann boundary conditions. Let* $M(u^+, u^-) = \mu - a_*(u^-)^2/(1+u^3)$ *for some constant* $a_* > 0$. *Then there exist thresholds* $0 < \Sigma_1 < \Sigma_2 < \infty$ *such that* $[0, \Sigma_j]^2$ *is invariant.*

If $u_0^\pm < \Sigma_1$ then $u^\pm$ tend to a spatially homogeneous distribution. In this case, Σ_1 is the critical mass below which no patterns form. The interaction induced turning rate λ in the preceeding lemma decreases to zero as the density increases to infinity. In our model, the maximal height of a ripple crest is fixed by the upper bound of the invariant domain. In the case of myxobacteria it is not known how the turning rates behave for extremely high densities. It is conceivable that the turning rates approach a positive constant. It would be helpful if more experiments about this behavior were carried out. Below, we introduce a turning functional which generalizes the one above and allows for a wider range of behavior.

Traveling wave patterns can be observed before the aggregation phase, and it was suggested that "rippling waves and the morphogenesis of fruiting bodies could both depend on the modulation of cell movement patterns by intercellular C-signaling" [19]. Therefore, we consider an example of a 'critical' turning rate where a slight change of parameters has a strong effect on the pattern forming behavior. We choose

$$\lambda(u^+, u^-) = \frac{a_*(u^-)^p}{1 + b_*(u^+ + u^-)^q}, \tag{20}$$

which for $p = 2, q = 3$ and $b_* = 1$ gives the situation studied above and for $p = q$ allows λ to approach a positive constant as the densities become large. The instability condition (11) becomes

$$\mu < \frac{a_*(p-1)c^p}{1 + b_*(2c)^q}, \tag{21}$$

which can be satisfied only if $p > 1$. So henceforth we assume this to be given. The domain $[0, s]^2$ is invariant if for $0 \le w \le s$ we have

$$\frac{s^p w - w^p s}{s - w} \le \frac{\mu}{a_*}(1 + b_*(s+w)^q). \tag{22}$$

The left hand side of (22) can be written as

$$\frac{s^{p+1} - w^{p+1}}{s - w} - (s^p + w^p). \tag{23}$$

By the mean value theorem we find

$$\frac{s^{p+1} - w^{p+1}}{s - w} = (p+1)\xi^p = \tilde{a}s^p \tag{24}$$

for some $\xi \in (w, s)$ and $1 < \tilde{a} \le p + 1$. So (22) is equivalent to

$$(\tilde{a} - 1)s^p \le \frac{\mu}{a_*}(1 + b_*(s+w)^q) + w^p. \tag{25}$$

The left hand side is bounded by ps^p, and hence, if $q > p$ then for all choices of parameters μ, a_*, b_* the invariance condition can be satisfied for large enough s. In case $p = q$ a necessary condition for invariant domains is $\tilde{a} - 1 \leq \mu b_*/a_*$ or equivalently $p \leq \mu b_*/a_*$. Next, suppose $q < p$ and let $w = s/2$. Then (25) becomes

$$s^p \leq \frac{\mu}{a_*(1 - 2^{1-p})} \left(1 + b_*(3/2)^q s^q\right). \tag{26}$$

This inequality is satisfied only for small s (and we already know that for small densities no rippling occurs), but cannot be satisfied for large s since s^p grows faster than s^q if $p > q$. The invariance condition does not hold in this case and we expect solutions to be unbounded. In the last section we use numerical simulations to investigate the behavior of the system for different parameter values.

2.2 Numerical simulations

Here we discuss simulations of (2) using the two types of turning functions as discussed above. First we consider

$$\lambda(u^+, u^-) = f(u^-) = 2 \tanh u^- \sqrt{u^-}. \tag{27}$$

This function grows superlinearly for some intermediate range of u^- and sublinearly for large arguments, but it is not bounded. It is plotted in Figure 2. Simulations are done using an explicit upwind scheme of first order which satisfies the CFL-condition [14]. Instead of taking Neumann boundary conditions we use the equivalent formulation given in Theorem 2.1 and consider periodic boundary conditions together with the symmetry condition for initial values. In particular, the implementation of boundary conditions does not influence the order of the scheme. Dropping the symmetry condition for the initial values (which is the same as dropping the no flux boundary conditions in the original formulation and results in enlarging the state space for the system) leads to different behaviors of the system, some of which have been described in [15]. We use 200 grid points. The value of autonomous turning is $\mu = 0.2$. Initial values are random perturbations of maximal value 0.01 of the constant homogeneous state $u^\pm = 0.5$. They are plotted as the zig-zag lines in Figure 2 (b). The shapes of $u^\pm$ after 80 000 time steps are also shown in Figure 2 (b). Each of the densities shows two peaks. The evolution of the ripples in time from the randomly perturbed homogeneous initial state can be seen for u^+ and u^- separately in Figure 3. Next we choose λ as in Lemma 2.5 with $a_* = 3$, i.e.,

$$\lambda(u^+, u^-) = a(u) f(u^-) = \frac{3}{1 + u^3} (u^-)^2. \tag{28}$$

The setting is as above, i.e., we have 200 grid points, $\mu = 0.2$, and initial values as random perturbations of the constant homogeneous stationary state. Only this time we use the Lax-Wendroff scheme which is formally of second order [24]. Figure 4 shows the initial and final (40 000 steps) profiles of the two densities $u^\pm$. This time five peaks develop in each direction. Figure 4 gives the time evolution of u^+ for 10 000 steps (a) and 40 000 steps (b).

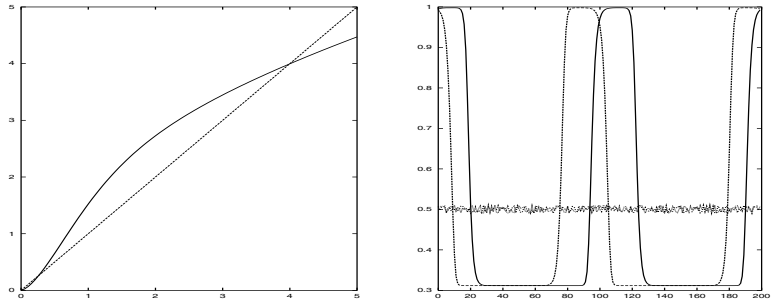

(a) (b)

Figure 2: The shape of f from (27) and the shapes of the two densities $u^{\pm}$ at the beginning and the end of the simulation.

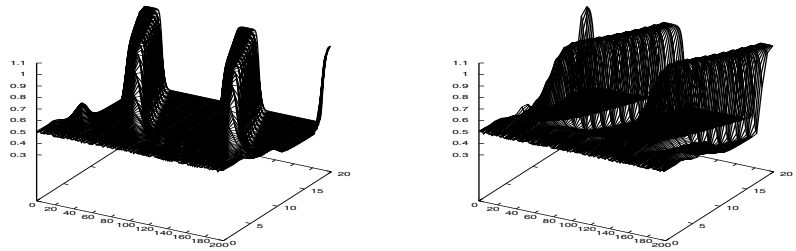

(a) (b)

Figure 3: The evolution of ripples from a perturbation of the stationary state with λ as in (27). The densities u^{+} (a) and u^{-} (b) are plotted every 4000 steps.

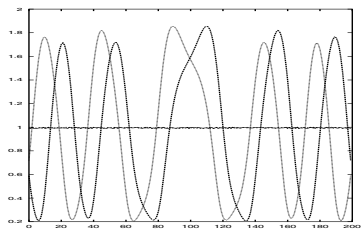

Figure 4: Initial and final density profiles of $u^{\pm}$ with λ as in (28).

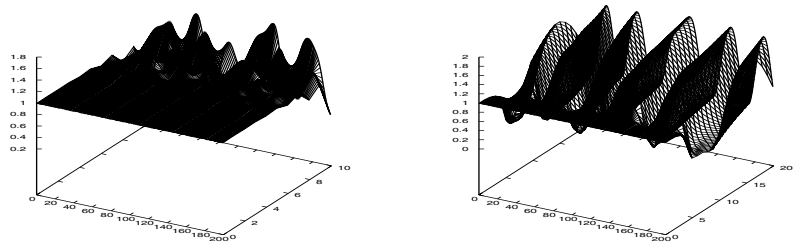

(a) (b)

Figure 5: The evolution of ripples from a perturbation of the stationary state with λ as in (28). The profile of u^+ is plotted for the first 10 000 time steps (a) and for 40 000 steps (b). The ripples appear stationary because of the choice of time steps between each plot.

3 A model for two different cell types

Here we extend the previous model to incorporate a second cell type. The two cell types differ in their intercellular signaling/response behavior as described in biological experiments, compare [19] . We assume that the two cell types have the same average speed γ and the same rate of autonomous turning μ. (It is obvious how to extend the model for different average speeds and autonomous turning rates). We denote the two densities by $u^{\pm}, z^{\pm}$ respectively. The model reads

$$\begin{aligned} u_t^+ + \gamma u_x^+ &= -(\mu + \lambda^+)u^+ + (\mu + \lambda^-)u^-, \\ u_t^- - \gamma u_x^- &= (\mu + \lambda^+)u^+ - (\mu + \lambda^-)u^-, \\ z_t^+ + \gamma z_x^+ &= -(\mu + \nu^+)z^+ + (\mu + \nu^-)z^-, \\ z_t^- - \gamma z_x^- &= (\mu + \nu^+)z^+ - (\mu + \nu^-)z^-, \end{aligned} \tag{29}$$

where $\lambda^{\pm}(u^+, u^-, z^+, z^-)$ and $\nu^{\pm}(u^+, u^-, z^+, z^-)$ are the respective turning rates induced by interaction.

We consider the case where the $z^{\pm}$-cells are genetically modified such that they are incapable of C-signaling, as described in [19]. Thus, contact with these cells does not induce reversal in other cells. One way to express this C-signaling deficiency of $z^{\pm}$-cells mathematically is to simply supress the $z^{\pm}$-dependence in the turning rates. We formulate a slightly more general approach which allows us to incorporate the total density of cells. Even though these mutant cells cannot induce reversal in other cells, their mere presence alters the probability of contact with a C-signaling capable cell at any point. Mathematically, saying that the turning rates depend only on $z = z^+ + z^-$ is the same as imposing the

following symmetry conditions:

$$\begin{aligned}\lambda^{\pm}(u^+,u^-,z^+,z^-) &= \lambda^{\pm}(u^+,u^-,z^-,z^+),\\ \nu^{\pm}(u^+,u^-,z^+,z^-) &= \nu^{\pm}(u^+,u^-,z^-,z^+).\end{aligned} \tag{30}$$

The symmetry condition (3) still holds and also applies to $\nu^{\pm}$:

$$\nu^+(u^+,u^-) = \nu^-(u^-,u^+) =: \nu(u^+,u^-). \tag{31}$$

We investigate the stability of the spatially homogeneous stationary state $u^{\pm} = c_1, z^{\pm} = c_2$. The linearized equations (the perturbations are also denoted by $u^{\pm}, z^{\pm}$) read

$$\begin{aligned}u_t^+ + \gamma u_x^+ &= \Lambda(u^- - u^+),\\ u_t^- - \gamma u_x^- &= \Lambda(u^+ - u^-),\\ z_t^+ + \gamma z_x^+ &= N(z^- - z^+) + \Theta(u^- - u^+),\\ z_t^- - \gamma z_x^- &= N(z^+ - z^-) + \Theta(u^+ - u^-),\end{aligned} \tag{32}$$

where

$$\begin{aligned}\Lambda &= \mu + \lambda + \partial_1\lambda c_1 - \partial_2\lambda c_1,\\ N &= \mu + \nu,\\ \Theta &= c_2(\partial_1\nu - \partial_2\nu),\end{aligned} \tag{33}$$

and all coefficient functions are evaluated at (c_1, c_1, c_2, c_2). The first two equations decouple from the last two. Therefore, the stability condition is similar to (6). The equations for $z^{\pm}$ can be used to determine the relation between the perturbations in $u^{\pm}$ and $z^{\pm}$.

Lemma 3.1 *The stationary solution $u^{\pm} = c_1 > 0, z^{\pm} = c_2 > 0$ of (2) is linearly stable if and only if*

$$\Lambda(c_1, c_1, c_2, c_2) > 0. \tag{34}$$

At the bifurcation point all eigenvalues cross the imaginary axis.

We now assume that the total density of cells is fixed but the relative amount of the two cell types varies. Let $c_1 = \beta c$, $c_2 = (1-\beta)c$ such that β is the fraction of cells which are capable of C-signaling. We furthermore assume, like in Section 2.1 case 2, that $\lambda(u^+,u^-,z^+,z^-) = a(u+z)f(u^-)$. (We do allow for a constant function a, i.e., Section 2.1 case 1.) Then the condition for instability is

$$a(2c)\left[f(\beta c) - f'(\beta c)\beta c\right] < -\mu. \tag{35}$$

By the modeling assumption we have $f(0) = 0$. If $f'(0)$ is bounded, then as β decreases to zero, condition (35) cannot be satisfied and hence the state is stable. This behavior corresponds well with the absence of rippling patterns for high densities of mutant cells, as observed in experiments [19] (compare also the next section). For $f(u^-) = (u^-)^2$, the instability condition is

$$\beta^2 > \frac{\mu}{a(2c)c^2}.$$

4 Ripple wavelength and viscosity

The linear analysis of (2) shows that when the homogeneous solution becomes unstable, all eigenvalues cross the imaginary axis. If in our original model we add some viscosity with parameter $\varepsilon > 0$, we can study the bifurcation behavior more closely. Viscosity terms are often used to account for terms of higher order (e.g. friction) which were neglected when deriving the equations . Equations (2) become

$$\begin{aligned} u_t^+ + \gamma u_x^+ &= \varepsilon u_{xx}^+ - \mu^+ u^+ + \mu^- u^-, \\ u_t^- - \gamma u_x^- &= \varepsilon u_{xx}^- + \mu^+ u^+ - \mu^- u^-. \end{aligned} \tag{36}$$

This system is of parabolic type. Standard theory gives (global) existence of (smooth) solutions [25] under relatively mild conditions on the turning rates. We first derive the dispersion relation which indicates a Hopf bifurcation. We also get a formula for the expected ripple wavelength. Then we show that limit sets of (36) are compact under suitable conditions on the turning rates. Instability of the homogeneous stationary state together with compactness of limit sets indicate that some kind of regular persisting patterns form, as was seen in the simulations.

The linearized equations with $u^\pm = c + w^\pm$ are

$$\begin{aligned} w_t^+ + \gamma w_x^+ &= \varepsilon w_{xx}^+ - \Lambda(w^- - w^+), \\ w_t^- - \gamma w_x^- &= \varepsilon w_{xx}^- - \Lambda(w^+ - w^-), \end{aligned} \tag{37}$$

where Λ is as in (6). Here we consider the interval $[0, 2l]$ with periodic boundary conditions and symmetry as before. We only allow perturbations with zero mass. An exponential ansatz for the perturbations $w^\pm$ results in eigenvalues $\xi_{1,2}$ as eigenvalues of the following matrix

$$\begin{pmatrix} -\varepsilon\frac{k^2\pi^2}{4l^2} - \Lambda - i\frac{k\pi\gamma}{2l} & \Lambda \\ \Lambda & -\varepsilon\frac{k^2\pi^2}{4l^2} - \Lambda + i\frac{k\pi\gamma}{2l} \end{pmatrix}. \tag{38}$$

Lemma 4.1 *The dispersion relation of system (36) on the interval* $[0, 2l]$ *with periodic boundary conditions is given by*

$$\xi_{1,2} = -\Lambda - \varepsilon\frac{k^2\pi^2}{4l^2} \pm \sqrt{\Lambda^2 - \frac{k^2\pi^2\gamma^2}{4l^2}}.$$

Hence, the stationary state $u^\pm = c$ *is linearly stable if and only if*

$$\Lambda > -\varepsilon\pi^2/4l^2. \tag{39}$$

We always assume $\varepsilon \ll \gamma$. For $\Lambda > 0$ the stationary state $u^\pm = c$ is stable as it was for $\varepsilon = 0$. As Λ decreases below zero the first bifurcation point is $\Lambda = -\varepsilon\pi^2/4l^2$ at which $\xi_1 = \bar{\xi}_2$ is purely imaginary. Hence, we expect a Hopf

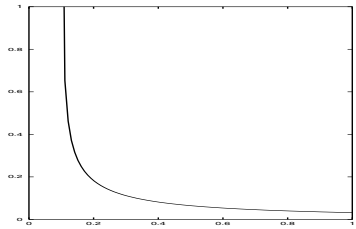

Figure 6: The wavelength l of ripples as a function of the fraction of C-signaling capable cells β given in (41) with $a = c = 1, \mu = 10^{-2}, \varepsilon\pi^2 = 10^{-3}$.

bifurcation. The minimal length of the interval for which such a bifurcation occurs can be interpreted as the wavelength of ripples. It is given by

$$l^2 = \frac{\varepsilon\pi^2}{-\Lambda}. \tag{40}$$

Now we are interested in the wavelength of ripples for the model with two cell types introduced in the previous section. We use the standard example $\lambda = a(u+z)(u^-)^2$ and denote by $c_1 = \beta c$ the fraction of cells which are capable of C-signaling. Then the ripple wavelength is

$$l^2 = \frac{\varepsilon\pi^2}{a(2c)c^2\beta^2 - \mu}. \tag{41}$$

Qualitatively, the shape of $l = l(\beta)$ is given in Figure 6. It closely resembles the curve found in experiments, [19].

Lemma 4.2 *Suppose the products $\lambda^\pm u^\pm$ are globally bounded. Then for all $\varepsilon > 0$ the limit set of any solution of (36) is compact in $\mathcal{C}([0,l])^2$. The case $\lambda = (u^-)^2/(1+u^3)$ is an example which satisfies the boundedness condition.*

Proof.
We write (36) in the new variables $u = u^+ + u^-$, $v = u^+ - u^-$ as

$$\begin{aligned} u_t + \gamma v_x &= \varepsilon u_{xx}, \\ v_t - \gamma u_x &= \varepsilon v_{xx} - 2\mu v + h(u,v), \end{aligned} \tag{42}$$

where, by assumption, $h(u,v) = 2(-\lambda^+ u^+ + \lambda^- u^-)$ is bounded by M, say. We work on $[0, 2l]$ with periodic boundary (and symmetry) condition. By successive use of partial integration we get

$$\frac{d}{dt}\int_0^{2l} u_x^2 + v_x^2 dx = -2\varepsilon \int_0^{2l} u_{xx}^2 + v_{xx}^2 dx - 4\mu \int_0^{2l} v_x^2 - 2\int_0^{2l} h(u,v) v_{xx} dx. \tag{43}$$

The last integral on the right hand side is estimated by the Cauchy-Schwarz and the Young inequality

$$\int h(u,v) v_{xx} dx \le M \int |v_{xx}| dx \le M\sqrt{2l}\sqrt{\int v_{xx}^2 dx} \le \frac{M^2 l}{2\varepsilon} + \varepsilon \int v_{xx}^2 dx. \tag{44}$$

Integrating

$$u_x(y) - u_x(x) = \int_x^y u_{xx}(s)ds$$

over $[0, 2l]$ and using the Cauchy-Schwarz inequality we get

$$|u_x(y)|l \leq \int_0^{2l} \int_x^y |u_{xx}|dsdx \leq 2l \int_0^{2l} |u_{xx}|dx \leq 2l\sqrt{2l}\sqrt{\int u_{xx}^2}.$$

A similar estimate holds for v. Integrating again with respect to x and multiplying by $-\varepsilon$ gives

$$-\varepsilon 4l^2 \int u_{xx}^2 + v_{xx}^2 dx \leq -\varepsilon \int u_x^2 + v_x^2 dx. \tag{45}$$

Inserting (45) and (44) into (43) results in

$$\frac{d}{dt}\int u_x^2 + v_x^2 dx \leq \frac{M^2 l}{2\varepsilon} - \frac{\varepsilon}{4l^2}\int u_x^2 + v_x^2 dx. \tag{46}$$

Therefore the integral $\int u_x^2 + v_x^2$ is bounded independently of t. The absolute values of u, v can be estimated by

$$|v(x)| \leq |u(x)| \leq \frac{\bar{u}}{l} + \sqrt{l}\sqrt{\int u_x^2 + v_x^2 dx}.$$

The imbeddings of $H^1(\Omega)^2$ into $L^2(\Omega)^2$ and $\mathcal{C}(\Omega)^2$ are compact so that trajectories are precompact in these spaces. Hence, the limit sets are nonempty and compact. ■

5 Formation of aggregates

In this last section we give an example of how our model (2) can be applied to another stage in the myxobacterial life cycle, namely to the aggregation phase. Under starvation conditions a large number of cells aggregate and form stalks which lift off the surface on which the bacteria had been moving. Finally, fruiting bodies develop. During the aggregation stage one finds bands of cells circling and spiralling around the center. These spiral patterns persist during the development of fruiting bodies. The formation of stalks is often preceeded by the rippling period. Starvation conditions induce differentiation of cells, which changes the pattern of protein synthesis [13]. The question of how such aggregates are held together and which forms of intercellular communication are necessary has been studied intensively.

One hypothesis is that trail following, together with the use of A-factor signaling, leads to stable aggregates. A-factor is not bound to the cell surface but diffuses from the cell and is supposed to act as a chemoattractant [13]. In a

cellular automaton model, [20, 23], it was shown that trail following is essential but not sufficient to keep aggregates together. Assuming that A-factor acts as a chemoattractant, the model accounted for stable aggregates of high densities.

In [26] it was suggested that instead of a chemoattractant there is a signal which "locks" cell motility to circling and spiralling behavior: once a cell is close to an aggregate it receives a signal which makes the cell stick to circling. Such a signal could be bound to the cell surface and transmitted by cell-cell contact.

The one dimensional model presented here can, of course, be only a caricature of the two or even three dimensional phenomenon. Analogous to being locked into circling, we consider here the possibility that cells become "locked into reversing" while moving in one space dimension. We suggest that due to differentiation, cells have a different response to cell-cell interaction and C-signaling. This response is captured in a turning function λ for which system (2) has no invariant domains. Hence, the densities can grow unboundedly. A cell which moves at the front edge of a small peak comes into contact with cells from a different peak moving in an opposite direction. It reverses its direction of movement due to C-signaling. It then moves opposite to the cells in the peak of which it was a member initially. C-signaling with those cells leads to reversing direction again (Figure 1). Repeated reversing makes cells almost immotile while new cells move towards the aggregate. A very simple turning function which captures this idea and gives blow-up like behavior is

$$\lambda(u^+, u^-) = a_*(u^-)^2 \tag{47}$$

for some sufficiently large parameter a_*. Note that (47) is a special case of the turning functional in (20) if we set $q = 0$ and rename the parameters. We use this function for simulations in Figure 7. We choose the special form for the initial values (7 (a)) so that one can follow the evolution of a single peak in detail. All simulations in this section are made using an upwind scheme, periodic boundary and the symmetry conditions.

We have seen two different behaviors of the system for the turning functional introduced in (20): existence of invariant domains for $q = 3, p = 2$ in Figure 5 and evolution of sharp peaks for $q = 0, p = 2$ in Figure 7. For the rest of this section we present some simulations on what happens when q varies between these two values and in particular around the critical value $q = p = 2$ discussed in Section 2.1.

We fix parameters $a_* = 3, b_* = 1, \mu = 0.2$ and $p = 2$. Initial values are random perturbations of maximal height 0.02 of the constant values $u^\pm = 1$. Figure 8 shows the formation of a sharp aggregate comparable to the one in Figure 7, but this time with arbitratily perturbed initial data and parameter $q = 1$.

Figure 9 shows the profiles of $u^\pm$ at the beginning of the simulation (the almost straight line of height one) and at the end (the peaks and patterns) for increasing q and increasing number of time steps of the simulation. In (a) we see the formation of a high aggregate for $q = 1.5$ after 4000 time steps, in (b) with $q = 1.8$ we still see the effect of "locking into turning" but even after 24 000 time

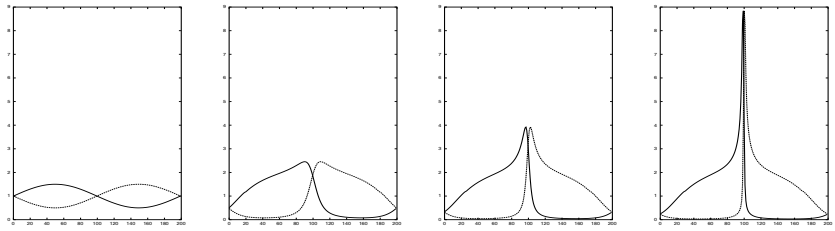

(a) (b) (c) (d)

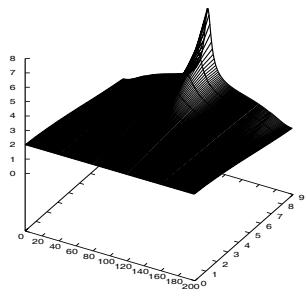

(e)

Figure 7: The profiles of $u^{\pm}$ during the development of a peak with λ as in (47). An upwind scheme with 200 grid points is used. Parameters are $a_* = 8, \mu = 0.1$. The plots are initial values (a), after 20 (b), 25 (c) and 30 (d) time steps. The time evolution of the total density $u = u^+ + u^-$ is given in (e).

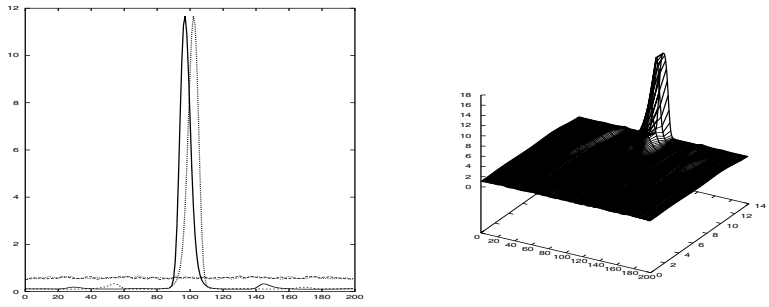

(a) (b)

Figure 8: Formation of aggregates with λ as in (20). Parameters are $a_* = 3, \mu = 0.2$ and $p = 2$, 2800 steps are computed. Initial values and final shapes of the densities are given in (a). The evolution of the total density $u = u^+ + u^-$ is shown in (b).

steps the densities are much lower than before. For $q = 2.2$ and $q = 2.5$ in (c) and (d) the densities after 40 000 time steps are clearly much lower than above, and in particular in (d) one sees the formation of plateaus, which indicates the existence of an invariant domain.

As we have seen, a slight change of parameters of the turning frequencies can change the behavior of ripple formation to the regime where aggregates are formed.

6 Discussion

The complex social behavior observed in myxobacteria requires intercellular signaling. C-factor is supposed to play an essential role in signaling and also in controlling movement behavior of individual cells. Since C-factor is bound to the cell surface, cells need to come into direct contact in order to transmit the signal. The question is what kind of behavior can be accounted for by direct interaction as opposed to long or moderate range of interaction through, for example, chemotaxis.

A simplified mathematical model for cell movement and local interaction was derived and investigated. Movement is confined to one spatial dimension. The model supports patterns which resemble rippling behavior. Qualitatively, the outcome of the model supports many experimental results like the critical mass of cells which is needed for rippling, and the influence that cells have on the ripple wavelength which are incapable of C-signaling. Finally, numerical simulations were shown to demonstrate the effect of "locking into turning". With a small parameter change in the turning frequencies, the rippling behavior could be

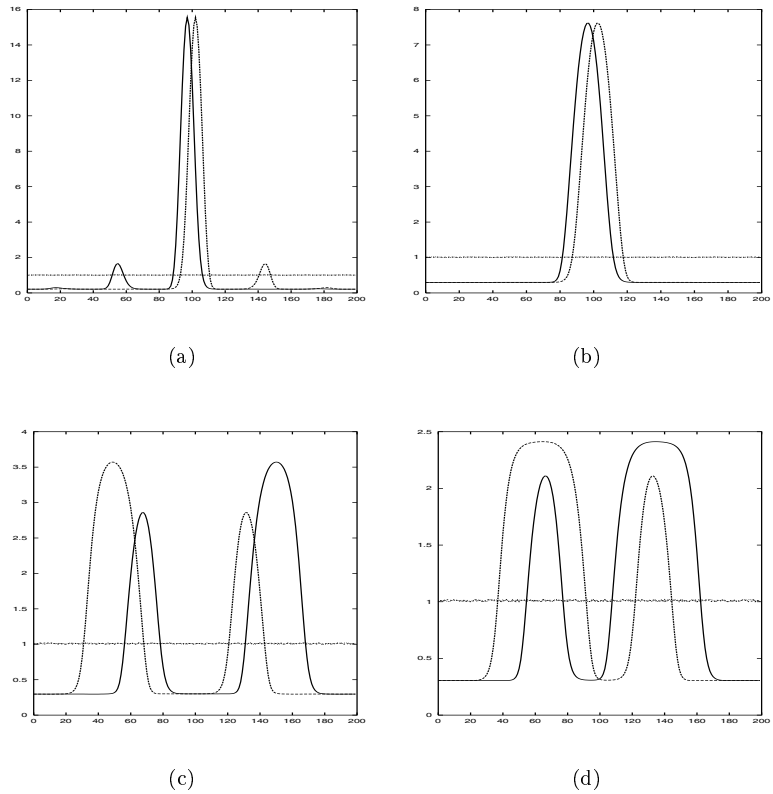

Figure 9: Emerging patterns with λ as in (20) for increasing q and increasing time interval. Parameters are $a_* = 3, b_* = 1, \mu = 0.2$ and $p = 2$. (a) has $q = 1.2$ and 4000 time steps, (b) has $q = 1.5$ and 24 000 time steps, (c) has $q = 2.2$ and 40 000 time steps and (d) has $q = 2.5$ and also 40 000 time steps. Note the different scales on the vertical axis. Whereas the maximum in (a) is almost 16 and in (b) almost 8, it is only about 3.5 in (c) and merely 2.5 in (b).

changed into the formation of aggregates. This is of special interest since the same genes in the C-signaling system are responsible for the stages of rippling and aggregation.

To describe rippling of myxobacteria, other models [2, 11] suggest the existence of an insensitive phase for each cell after reversal. If there is no such phase, as assumed in the present paper, then the average free path length in crests should be smaller than in troughs. Sager and Kaiser indicated in their experiment of tracking flourescently labelled cells whether these cells were in crests or troughs. The results are shown in Figure 6B, [19]. On first sight, paths in crests cover less distance, but no analysis was done to confirm this impression. Further detailed statistics on the length of the paths would be desirable.

Acknowledgement: The second author thanks Dale Kaiser (Stanford University) for the frequent and patient discussions about pattern formation in myxobacteria.

References

[1] B.D. Blackhard and D.R. Zusman. "frizzy" genes of myxococcus xanthus are involved in control of frequency of reversal of gliding motility. *Proc. Natl. Acad. Sci. USA*, 82:8767–8770, 1995.

[2] U. Börner, A. Deutsch, H. Reichenbach, and M. Bär. Rippling in myxobacterial aggregates - patterns arising from cell-cell collisions. *Preprint, Max Planck Institut, Dresden*, 2001.

[3] E. Geigant. *Nichtlineare Integro-Differential-Gleichungen zur Modellierung von Musterbildungsprozessen auf S^1*. PhD thesis, Universität Bonn, 1999.

[4] E. Geigant, K. Ladizhansky, and A. Mogilner. An integro-differential model for orientational distributions of f-actin in cells. *SIAM J. Appl. Math.*, 59:787–809, 1999.

[5] K.P. Hadeler. Random walk systems and reaction telegraph equations. In S. v. Strien and S.V. Lunel, editors, *Dynamical Systems and their Applications in Science*. Royal Academy of the Netherlands, 1996.

[6] K.P. Hadeler. Reaction transport systems in biological modelling. In V. Capasso and O. Diekman, editors, *Mathematics Inspired by Biology*, Lect. Notes Math. 1714, pages 95–150, Heidelberg, 1999. Springer Verlag.

[7] T. Hillen. A Turing model with correlated random walk. *J. Math. Biol.*, 35:49–72, 1996.

[8] T. Hillen. Invariance principles for hyperbolic random walk systems. *J. Math. Ana. Appl.*, 210:360–374, 1997.

[9] T. Hillen, C. Rohde, and F. Lutscher. Existence of weak solutions for a hyperbolic model for chemosensitive movement. *J. Math. Anal. Appl.*, 260:173–199, 2001.

[10] T. Hillen and A. Stevens. Hyperbolic models for chemotaxis in 1-D. *Nonlinear Analysis: Real World Applications*, 1:409–433, 2000.

[11] O. Igoshin, A. Mogilner, R. Welch, D. Kaiser, and G. Oster. Pattern formation and traveling waves in myxobacteria: Theory and modeling. *Proc. Natl. Acad. Sci.*, to appear.

[12] M. Kac. A stochastic model related to the telegrapher's equation. *Rocky Mountain J. Math.*, 4:497–509, 1956.

[13] D. Kaiser and L. Kroos. Intercellular signaling. In Kaiser Dworkin, editor, *Myxobacteria II*, Washington, DC, 1993. American Society for Microbiology.

[14] R. LeVeque. *Numerical Methods for Conservation Laws.* Birkhäuser, Basel, 1992.

[15] F. Lutscher. *Modeling moving polarized groups of animals and cells.* PhD thesis, Universität Tübingen, 2000 . `http://w210.ub.uni-tuebingen.de/dbt/volltexte/2000/203`.

[16] F. Lutscher. Modeling alignment and movement of animals and cells. *J. Math. Biol.*, accepted.

[17] M.J. McBride, P. Hartzell, and D.R. Zusman. Motility and tactic behavior of myxococcus xanthus. In Kaiser Dworkin, editor, *Myxobacteria II*, Washington, DC, 1993. American Society for Microbiology.

[18] B. Pfistner. A one dimensional model for the swarming behavior of Myxobakteria. In W. Alt and G. Hoffmann, editors, *Biological Motion.* Lect. Notes on Biomath., 89, Springer, 1990.

[19] B. Sager and D. Kaiser. Intercellular c-signaling and the traveling waves of myxococcus. *Genes & Development*, 8:2793–2804, 1994.

[20] A. Stevens. Simulations of the gliding behavior and aggregation of myxobacteria. In W. Alt and G. Hoffmann, editors, *Biological Motion*, pages 548–555. Lect. Notes on Biomath., 89, Springer, 1990.

[21] A. Stevens. Trail following and aggregation of myxobacteria. *J. Biol. Systems*, 3(4):1059–1068, 1995.

[22] A. Stevens. The derivation of chemotaxis-equations as limit dynamics of moderately interacting stochastic many particle systems. *SIAM J. Appl. Math.*, 61(1):183–212, 2000.

[23] A. Stevens. A stochastic cellular automaton, modeling gliding and aggregation of myxobacteria. *SIAM J. Appl. Math.*, 61(1):172–182, 2000.

[24] J. Strickwerda. *Finite difference schemes and partial differential equations.* Chapman & Hall, New York, 1989.

[25] M.E. Taylor. *Partial Differential Equations III.* Springer, New York, 1996.

[26] D. White. Myxospore and fruiting body morphogenesis. In Kaiser Dworkin, editor, *Myxobacteria II*, Washington, DC, 1993. American Society for Microbiology.